State-dependent cloud phase feedback makes equilibrium climate sensitivity > 5°C plausible

Jenny Bjordal[1], Trude Storelvmo[1,2,*], Kari Alterskjær[2,3], Tim Carlsen[1]

[1] Department of Geoscience, University of Oslo, Oslo, Norway
[2] Nord University, Bodø, Norway
[3] Center for International Climate and Environmental Research–Oslo (CICERO), Oslo, Norway
[*] Corresponding author

Earth's equilibrium climate sensitivity (ECS) measures how much the global mean surface air temperature will ultimately increase for a doubling of atmospheric carbon dioxide (CO_2) and has become the standard metric to quantify how sensitive Earth's climate is to atmospheric greenhouse gas perturbations. For decades, global climate models (GCMs) have produced ECSs between approximately 2 and 4.5°C, but interestingly, that is about to change: a large subset of GCMs participating in the ongoing 6th coupled model intercomparison project (CMIP6) is producing ECSs well above 5°C. The latest version of the Community Earth System Model, CESM2[1], is an example of such a high-ECS model. It reproduces the historical temperature record well despite its high ECS, contrary to what has previously been considered possible[2]. This can be explained by the fact that CESM2 has a net positive cloud-climate feedback that grows with time - the warmer it gets, the more clouds change in a way that further amplifies the warming, while for modest warming this amplification is much smaller. We have identified the physical mechanism responsible for this transition to a high-sensitivity climate state in CESM2 and argue that our findings demand a re-evaluation of prior observational constraints on ECS. Further, we argue that while the exact timing and magnitude of the transition may be model dependent, its existence is undisputable, and the associated policy-implications are wide-reaching.

Cloud feedbacks, i.e. the extent to which clouds amplify or dampen perturbations to Earth's climate, represent the largest source of uncertainty in estimating the climate sensitivity in GCMs[3]. Clouds come in many flavours and respond differently to warming depending on their type and characteristics – for example, high tropical ice clouds tend to rise to higher altitudes[4], while the amount of low subtropical clouds is expected to reduce, with warming[5]. These two well established warming-induced cloud changes both represent positive (amplifying) feedbacks[6].

There are multiple ways to categorize clouds, depending on the feedback mechanism of interest. For example, we can divide them according to their thermodynamic phase; mixed-phase clouds contain a mixture of ice and liquid, and are found between 0 and approximately -38°C. These clouds have a strong influence on Earth's energy budget, especially at high latitudes, and are most abundant over the Southern Ocean[7]. It has been known for decades that water droplets tend to be more numerous and smaller than ice crystals, and that liquid clouds will therefore reflect much more solar radiation than an otherwise similar ice cloud[8]. As a consequence of this, clouds with higher supercooled liquid fractions (SLFs, the ratio of liquid to total cloud condensate) will generally be optically thicker and thus reflect more solar radiation back to space. As the Earth warms, we expect the phase composition in clouds to change such that SLF increases, contributing to a negative (damping) cloud feedback[9].

Gettelman et al.[10] recently found that the increase in ECS from 4.0°C in CESM1 to 5.3°C in CESM2 was mostly due to cloud feedbacks. They further stated that while it remains unclear how plausible such a high climate sensitivity is, CESM2 has an improved cloud distribution and compares better to observations than its predecessor CESM1[10].

To further investigate the high ECS in CESM2 we have looked into its overall cloud feedback by decomposing it into feedbacks associated with cloud altitude, amount and optical depth changes.

Here we present these feedbacks and discuss the mechanism responsible for CESM2's gradual transition to a high climate sensitivity state with warming.

To evaluate the ECS and the cloud feedbacks we used the fully coupled CESM2 with the Cloud Feedback Model Intercomparison Project (CFMIP) Observation Simulator Package (COSP)[11] enabled. Note that the simulations here have a different horizontal resolution and somewhat higher ECS than those in Gettelman et al. (2019) (see Methods). Following the standard procedure of calculating ECS[12], we forced the simulation with an abrupt quadrupling of atmospheric carbon dioxide concentration from pre-industrial conditions. From this simulation and a control simulation we decomposed the cloud feedbacks by using radiative kernels following Zelinka et al.[13].

Despite the high ECS of the CESM2 simulations presented here (6.8°C with an 95% uncertainty range from 6.5 to 7.1°C), the historical temperature evolution remains well represented and generally lies within the observational uncertainty (Figure 1a). Figure 1b shows the simulated temporal evolution of surface air temperature after CO_2 quadrupling, which already after 150 years of simulation approaches 9°C, driven by a radiative energy imbalance (EI) at the top-of-the-atmosphere (TOA) induced by the CO_2 quadrupling. Initially, the EI decreases rapidly with warming, but after 10-15 years this rate of decrease slows considerably, resulting in an EI which after 150 years remains large at approximately 2.5 Wm^{-2}. This is also evident from Figure 1c, which shows a regression of EI against the global mean surface air temperature (SAT) change. The slope of this regression gives the feedback parameter while the inferred ECS is obtained by dividing the intercept of the regression line with the x-axis by two[14]. A regression over the first 15 years of the simulation results in a steeper slope and thus a weaker inferred ECS[14]while using the full simulation results in a larger inferred ECS. The latter is currently the standard method of calculating ECS[3]. The difference between the two regression lines indicates that the overall climate feedback changes over the 150-year simulation period. Figure 1c further shows that the reason the EI is far from zero even after 150 years of simulation is that the climate system increasingly absorbs more shortwave (SW) radiation with warming over time, which compensates for much of the warming-induced increase in outgoing longwave (LW) radiation to space (the well-known Planck feedback). Figure 1d shows that cloud changes that amplify with time can largely explain the weak reduction of the EI with warming.

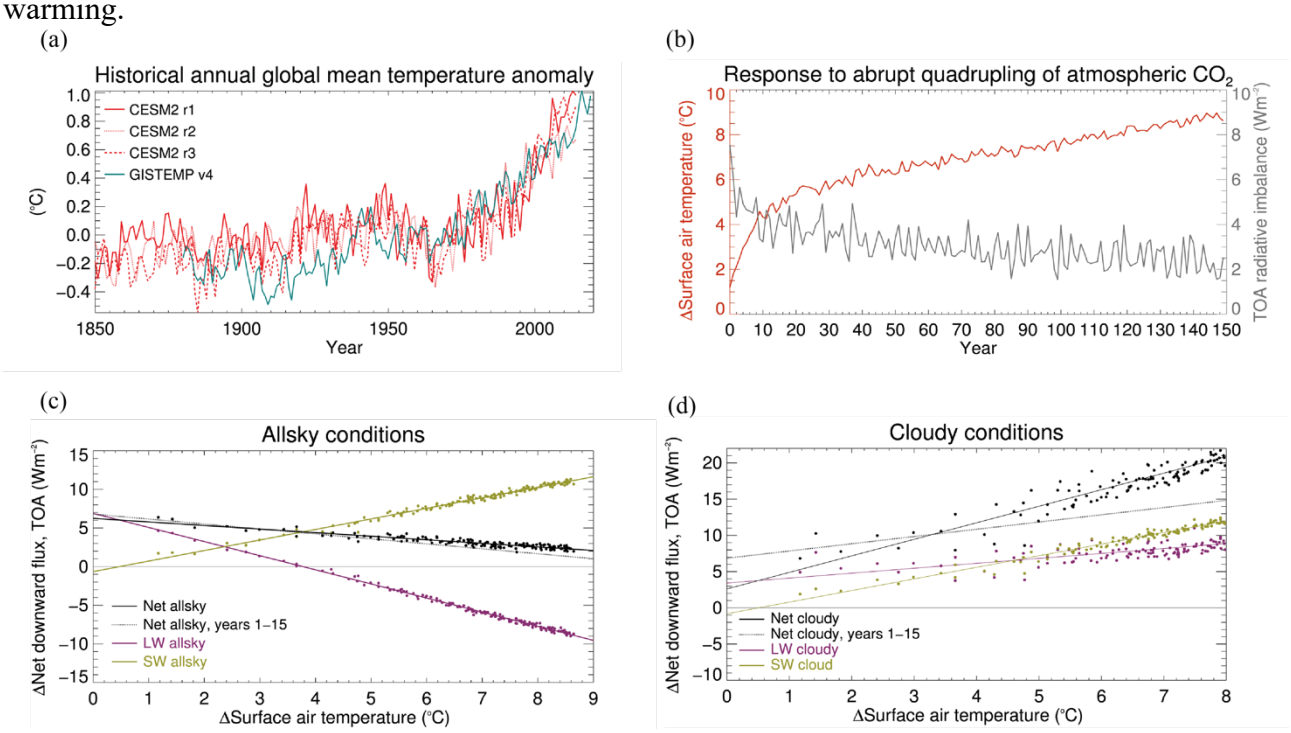

Figure 1: Near surface temperature and radiative responses to a quadrupling of atmospheric CO_2. (a) Historical global mean near surface temperature evolution from observations (GISTEMP v4) and three ensemble members of CESM2 (b) Change in near surface temperature (K) and TOA radiative imbalance (W m^{-2}) development between a

simulation of abrupt atmospheric CO_2 quadrupling (4xCO2) and a control simulation. (c) Dots show global annual-mean changes in TOA downward radiative flux under "all-sky" conditions against the corresponding global annual-mean change in near surface temperature between the 4xCO2 and the control simulations. Lines show linear regression fits to the data, where the slope and the intercept gives the feedback parameter (W m^{-2} K^{-1}) and the effective radiative forcing (W m^{-2}), respectively. Net flux changes are shown in black, longwave (LW) in purple and shortwave (SW) in green. The dotted grey line shows a regression where only the first fifteen years of the net all-sky conditions are utilised. (d) As in (c), but for cloudy conditions only.

To further demonstrate how cloud changes influence the EI over time, Figure 2a shows the net cloud feedback evolution over the simulated 150 years post CO_2 quadrupling. Evident is a cloud feedback that is initially large and positive, but which thereafter grows with time. This cloud feedback increase is responsible for the transition in CESM2 from a medium-ECS state under historical and present-day conditions, to an extremely high-ECS state for warming beyond 3-4°C (feedbacks as a function of SAT change are shown in Figure S1). Figures 2a further shows that it is mainly a change in the feedback associated with cloud optical depth changes that drives the overall cloud feedback change (~63%), with smaller contributions from changes in cloud altitude (~21%) and amount (~16%). Figures 2b and 2c show that the net cloud feedback changes stem primarily from changes to the shortwave cloud feedback.

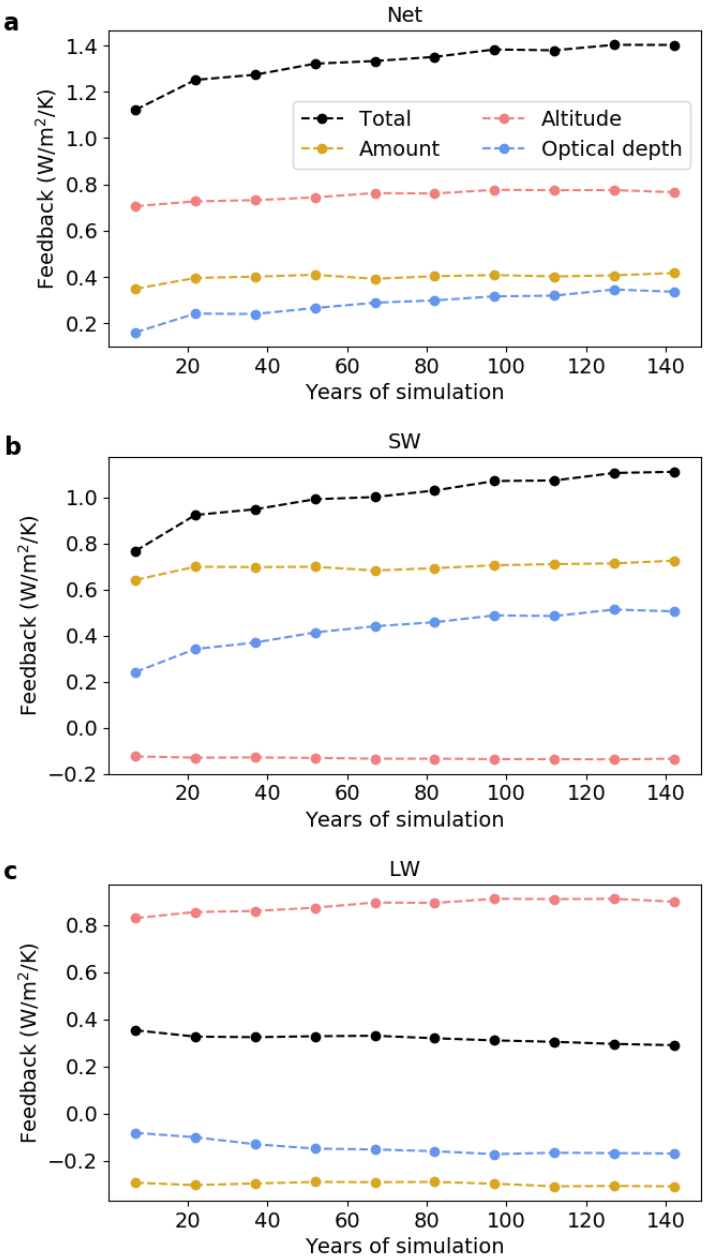

Figure 2: Total and decomposed cloud feedbacks with time. 15-year average net (a), SW (b) and LW (c) cloud feedbacks for the 150 years of the CESM2 simulation after quadrupling of CO_2. Dots are placed at the middle of each 15-year interval, for the total cloud feedback (black) and separated into the cloud amount feedback (yellow), the cloud altitude feedback (red) and the cloud optical depth feedback (blue).

From the maps shown in Figure 3 we can see that most of this change in the optical depth feedback occurs over the Southern Ocean (though notable changes occur also in the Arctic and the Southeast Pacific). The importance of the different latitude regions for the overall feedback change is also shown in figure S2. Early in the 150-year simulation, the zonal mean optical depth feedback is generally positive at low latitudes (linked to dehydration of the low-cloud layer with warming), and negative at mid- to high latitudes, particularly in the Southern Ocean. Mixed-phase clouds are abundant in this region, which therefore has a large potential for a negative optical depth feedback, as evident in Figure 3a (45-60°S mean of -1.25 Wm^{-2} K^{-1}). However, towards the end of the simulation, the negative optical depth feedback in the Southern Ocean has virtually vanished (-0.02 Wm^{-2} K^{-1}, Figure 3b).

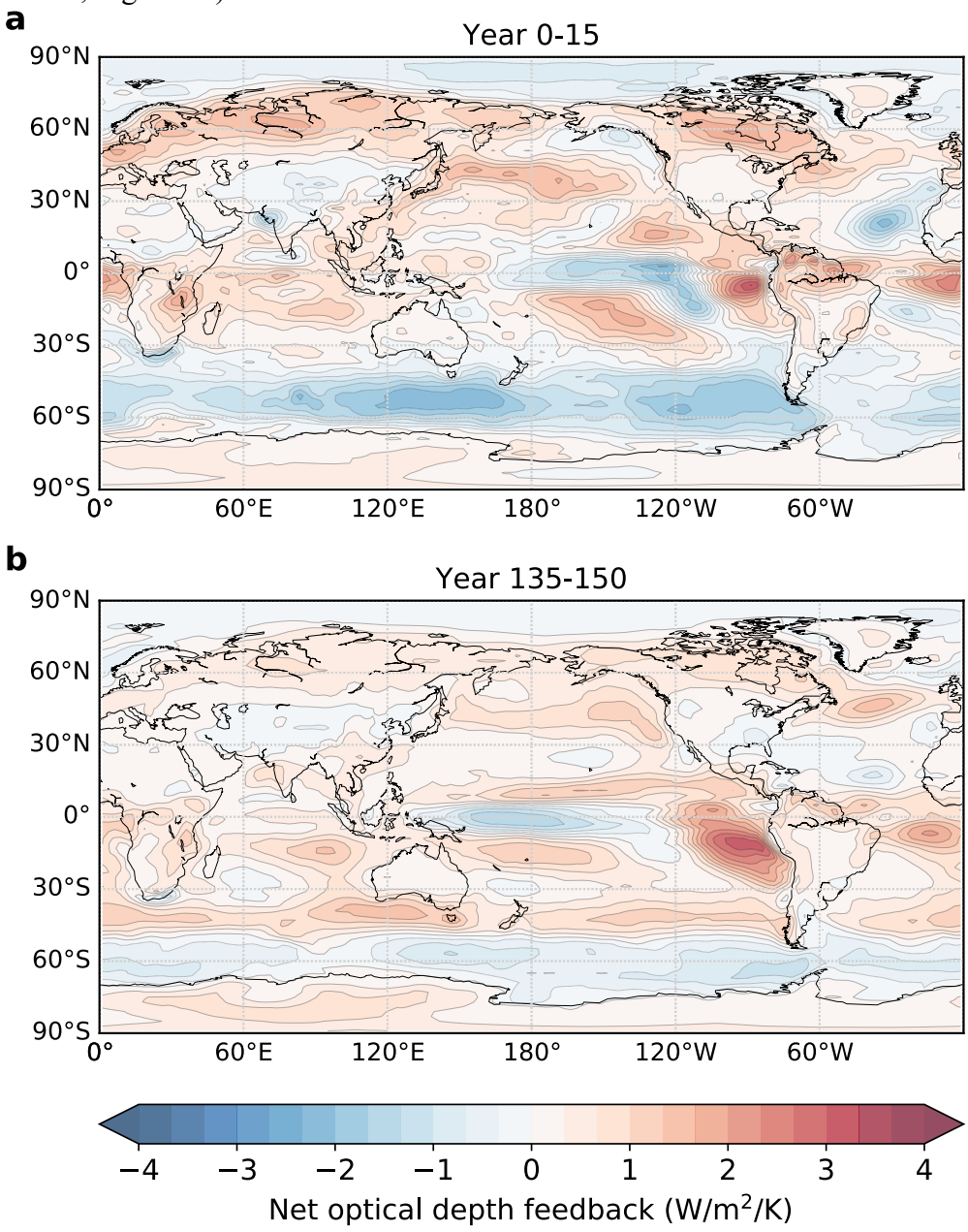

Figure 3: Maps of the net optical depth feedback at the beginning and end of the simulation.
The spatial distribution of the net optical depth feedback ($Wm^{-2}K^{-1}$) for the first (a) and the last (b) 15 years of the 150-year simulation following a quadrupling of CO_2 simulation with CESM2.

The increase in optical depth feedback over the Southern Ocean can be explained by the following mechanism: As the temperature increases, more of the Southern Ocean clouds become liquid and fewer consist of ice, which increases their optical thickness. The increase in optical thickness in turn reduces the warming, giving the negative feedback that we see over the Southern Ocean early in the simulation. The existence of a negative cloud feedback over the Southern Ocean has been confirmed observationally from space[15], and the magnitude of the feedback in CESM2 appears to be consistent with that inferred from these satellite observations (95% confidence interval for 45-60°S of -1.7 to -0.1 Wm^{-2} K^{-1}). However, as the temperature increases, eventually most clouds in the Southern Ocean will already be liquid and no further phase-related changes to cloud optical depth can occur. This results in a weakening of the negative Southern Ocean feedback as the temperature increases, causing the overall global (positive) cloud feedback to increase with time. As evident from Figure 4, the fractional content of ice within the clouds over the Southern Ocean clearly decreases as the atmosphere warms. The decrease is largest in the lower troposphere where the average temperature increases to be above 0°C, moving the mixed-phase cloud region upwards. This is also the altitude range in which we find most of the cloud water (measured in mass mixing ratios) in the region (Figure 4).

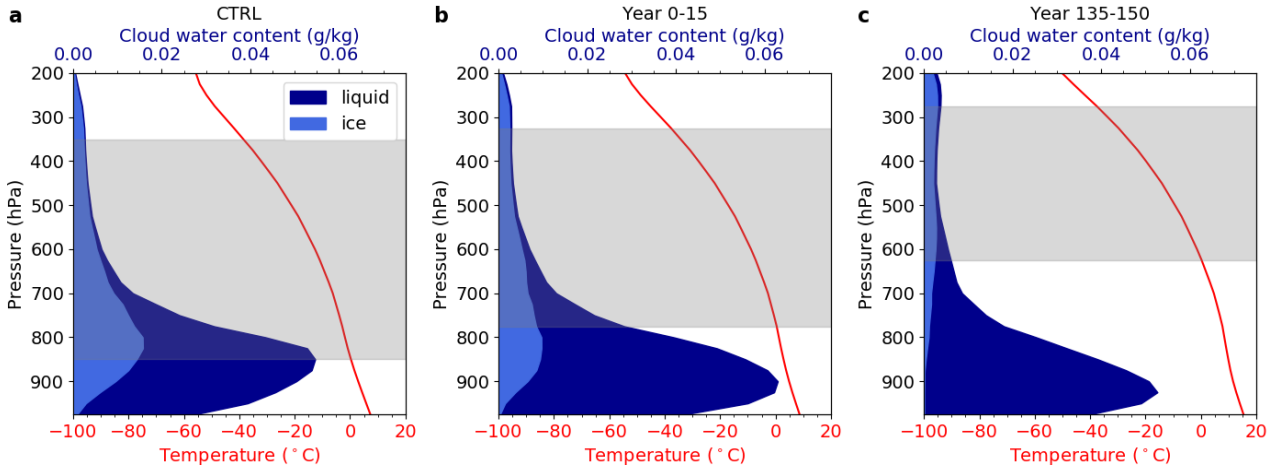

Figure 4: Cloud water and temperature profiles for summer over the Southern Ocean.
The summer (DJF) grid-box average of cloud water amount and temperature profiles (red lines) for the pre-industrial control simulation (a) the first 15 years (b) and the last 15 years (c) of the 150-year simulation with quadrupling of CO_2. The ice fraction is light blue and the liquid fraction in dark blue. The mixed-phased cloud region (temperatures between 0 and -38°C) is shown in grey shading.

This confirms that the low clouds over the Southern Ocean are over the 150-year simulation approaching a state where almost all the ice in the clouds is gone, particularly for the part of the year when the amount of solar radiation reflected back to space is most susceptible to cloud changes (December-February is shown in Fig. 4, see Figures S3-S5 for other seasons). Figure S6 shows that CESM2 has vertical profiles of total cloud water, phase partitioning and temperature which are broadly consistent with atmospheric reanalyses and active spaceborne remote sensing[16,17].

We argue that the mechanism described above must operate, and thus the optical depth feedback should change with warming both in reality and in other GCMs. However, exactly how important this effect becomes depends crucially on the amount of warming in the Southern Ocean region, and is thus tightly interlinked with other (cloud) feedbacks. Intuitively, GCMs that have more ice in mixed-phase clouds initially, will also require more warming for the transition to a high-sensitivity state to occur, because the optical depth feedback starts out much more negative over the Southern Ocean. Too low SLF was a known problem for many of the CMIP5 models [18,19], as was a large bias in the optical depth of Southern Ocean clouds[20]. These biases have been corrected in many of the CMIP6 models[21,10], and thus it is very likely that the demonstrated increase in cloud feedbacks seen in CMIP6 models relative to CMIP5 can be explained by a weaker negative cloud phase feedback.

This is corroborated by the fact that the increased cloud feedback in CMIP6 has been traced back to extratropical clouds, and primarily to the Southern Ocean[22].

While the idea of state-dependent cloud feedbacks is not new[23 24], the literature has so far focused on tropical cloud feedbacks. In contrast, the results presented here support a strong state-dependence of feedbacks operating in extratropical clouds, that is particularly prevalent in the Southern Hemisphere. The existence of a strong negative cloud feedback at present, that retards warming in the Southern Ocean, may well have played an important role in the considerable hemispheric asymmetry in surface air temperature increase seen over the last century[25], and potentially also in the observed sluggish rate of Antarctic sea ice loss so far. This has so far primarily been attributed to the fact that it takes centuries for a global warming signal to emerge in the deep ocean waters upwelling in this region[26]. There is now recent evidence from multi-century GCM simulations that ocean processes that govern the emergence of Southern Ocean surface warming may control the triggering of the cloud phase feedback weakening[27], thus highlighting the urgency of understanding how both mechanisms operate and interact in nature as well as in the latest generation of GCMs. Recent indications that Antarctic and Southern Ocean climate change is accelerating[28] further underscore this urgency.

METHODS

In the comparison of observed historical surface air temperature with that of CESM2 ensemble members (Figure 1a), the CESM2 data (from simulations at approximately 2 by 2 degree resolution) was downloaded from the CMIP6 archive (date of download from the Earth System Grid Federation: April 3rd 2020), while observations were taken from the GISTEMP v4 data set[29 30]. The spread of CESM2 ensemble members illustrates uncertainty related to natural variability, while observational uncertainty is on the order of 0.2°C (95% confidence interval) in the early 1900s, reducing to near 0.05°C for the last 50 years[29].

The change in TOA downward radiative flux and near surface air temperature shown in Figure 1(b-d) is calculated based on CESM2 simulations performed by the authors (same horizontal resolution, but with COSP enabled), by taking the global annual-mean values of a 150-year 4xCO2 simulation and subtracting a linear regression of the values in the corresponding time segment of a control simulation following Forster et al.[31]. This method removes any drift from remaining energy imbalance in the control simulation from the analysis. The linear regressions of Figure 1c show what is commonly referred to as the "Gregory estimates" following e.g. Gregory et al.[14], Forster et al.[31] and Andrews et al.[32]. The effective radiative forcing (W m^{-2}) is given by the regression line y-axis intercept, the effective climate sensitivity is found by dividing the x-axis intercept by two and the slope of the line gives the climate feedback parameter (W m^{-2} K^{-1}). The effective climate sensitivity is found to be 6.76°C (95% confidence interval of 6.50 – 7.07, produced based on bootstrapping using 3000 realizations). Figure 1d shows the true (all-sky) radiative contribution from cloudy conditions.

The comparison between CESM2 and spaceborne remote sensing shown in Figure S6 uses satellite-retrieved liquid water content (LWC) and ice water content (IWC) data that stem from observations with the Cloud Profiling Radar (CPR) on CloudSat[16] and the Cloud-Aerosol Lidar with Orthogonal Polarization (CALIOP)[17] on CALIPSO between June 2006 and March 2011. The LWC profiles from the CloudSat Radar-Only Cloud Water Content Product[33] (2B-CWC-RO version P1_R05, variable 'RO_liq_water_content') and the IWC profiles from the CloudSat and CALIPSO Ice Cloud Property Product[34,35] (2C-ICE version P1_R05, variable 'IWC') are complemented by atmospheric temperature and pressure profiles from the ECMWF-AUX data set (version P_R05) that contains ancillary European Center for Medium-Range Weather Forecast (ECMWF) state variable data interpolated to each CPR bin. Each LWC, IWC, and temperature profile over the Southern Ocean (45-60°S) is re-gridded on a common pressure grid using nearest-neighbour interpolation to facilitate along-track averaging. The LWC and IWC data (kg m^{-3}) are screened using the provided

quality flags and converted to mixing ratios (kg/kg) by means of the air density calculated from the pressure and temperature data for each bin. Finally, the seasonal and annual averages for all-sky conditions in the Southern Ocean region are computed between 2006 and 2011. Note that the radar reflectivity strongly depends on the particle size of the hydrometeors and, thus, is influenced by precipitation particles. For the comparison with CESM2, the simulated IWC and LWC profiles shown in Fig. S6 additionally include snow and rain (in contrast to the profiles shown in Fig. 4). For the satellite retrieval, uncertainties for LWC and IWC are included in the satellite products for each individual profile. They are mostly in the order of 20 to 40 %, varying considerably with altitude and atmospheric conditions. The given error estimates were propagated in the calculation of the averaged LWC and IWC profiles. As several hundred thousand of profiles are averaged over the SO region each month, the propagated error becomes negligible.

AUTHOR CONTRIBUTIONS:

JB ran all model simulations, performed most of the analysis, produced figures 2-4, and helped write the paper. TS designed the study and wrote the paper with help from all authors. KA performed analysis, produced Figure 1 and helped write the paper, and TC performed the observational analysis that went into Figure S3 and helped write the paper.

ACKNOWLEDGEMENT:

This work was supported by the European Research Council (ERC) through Grant StG 758005, and by the Norwegian Research Council through grant 281071.

REFERENCES:

1. Danabasoglu, G. *et al.* The Community Earth System Model Version 2 (CESM2). *J. Adv. Model. Earth Syst.* (2020). doi:10.1029/2019MS001916
2. Otto, A. *et al.* Energy budget constraints on climate response. *Nature Geoscience* (2013). doi:10.1038/ngeo1836
3. Flato, G. *et al.* IPCC 2013 AR5 - Chapter 9: Evaluation of Climate Models. *Clim. Chang. 2013 Phys. Sci. Basis. Contrib. Work. Gr. I to Fifth Assess. Rep. Intergov. Panel Clim. Chang.* (2013). doi:10.1017/CBO9781107415324
4. Zelinka, M. D. & Hartmann, D. L. Why is longwave cloud feedback positive? *J. Geophys. Res. Atmos.* (2010). doi:10.1029/2010JD013817
5. Sherwood, S. C., Bony, S. & Dufresne, J. L. Spread in model climate sensitivity traced to atmospheric convective mixing. *Nature* (2014). doi:10.1038/nature12829
6. Gettelman, A. & Sherwood, S. C. Processes Responsible for Cloud Feedback. *Current Climate Change Reports* (2016). doi:10.1007/s40641-016-0052-8
7. Matus, A. V. & L'Ecuyer, T. S. The role of cloud phase in Earth's radiation budget. *J. Geophys. Res.* (2017). doi:10.1002/2016JD025951
8. Mitchell, J. F. B., Senior, C. A. & Ingram, W. J. CO2 and climate: A missing feedback? *Nature* (1989). doi:10.1038/341132a0
9. Tan, I., Storelvmo, T. & Zelinka, M. D. Observational constraints on mixed-phase clouds imply higher climate sensitivity. *Science (80-.).* (2016). doi:10.1126/science.aad5300
10. Gettelman, A. *et al.* High Climate Sensitivity in the Community Earth System Model Version 2 (CESM2). *Geophys. Res. Lett.* (2019). doi:10.1029/2019gl083978
11. Bodas-Salcedo, A. *et al.* COSP: Satellite simulation software for model assessment. *Bull. Am. Meteorol. Soc.* (2011). doi:10.1175/2011BAMS2856.1
12. Eyring, V. *et al.* Overview of the Coupled Model Intercomparison Project Phase 6 (CMIP6) experimental design and organization. *Geosci. Model Dev.* (2016). doi:10.5194/gmd-9-1937-2016
13. Zelinka, M. D., Klein, S. A. & Hartmann, D. L. Computing and Partitioning Cloud

Feedbacks Using Cloud Property Histograms. Part I: Cloud Radiative Kernels. *J. Clim.* 3715–3735 (2012). doi:10.1175/JCLI-D-11-00248.1
14. Gregory, J. M. *et al.* A new method for diagnosing radiative forcing and climate sensitivity. *Geophys. Res. Lett.* **31**, 2–5 (2004).
15. Ceppi, P., McCoy, D. T. & Hartmann, D. L. Observational evidence for a negative shortwave cloud feedback in middle to high latitudes. *Geophys. Res. Lett.* (2016). doi:10.1002/2015GL067499
16. Stephens, G. L. *et al.* THE CLOUDSAT MISSION AND THE A-TRAIN. *Bull. Am. Meteorol. Soc.* (2002). doi:10.1175/bams-83-12-1771
17. Winker, D. M. *et al.* The Calipso Mission: A Global 3D View of Aerosols and Clouds. *Bull. Am. Meteorol. Soc.* (2010). doi:10.1175/2010BAMS3009.1
18. Cesana, G., Waliser, D. E., Jiang, X. & Li, J. L. F. Multimodel evaluation of cloud phase transition using satellite and reanalysis data. *J. Geophys. Res.* (2015). doi:10.1002/2014JD022932
19. Komurcu, M. *et al.* Intercomparison of the cloud water phase among global climate models. *J. Geophys. Res.* (2014). doi:10.1002/2013JD021119
20. Hyder, P. *et al.* Critical Southern Ocean climate model biases traced to atmospheric model cloud errors. *Nat. Commun.* (2018). doi:10.1038/s41467-018-05634-2
21. Bodas-Salcedo, A. *et al.* Strong Dependence of Atmospheric Feedbacks on Mixed-Phase Microphysics and Aerosol-Cloud Interactions in HadGEM3. *J. Adv. Model. Earth Syst.* **11**, 1735–1758 (2019).
22. Zelinka, M. D. *et al.* Causes of Higher Climate Sensitivity in CMIP6 Models. *Geophys. Res. Lett.* **47**, (2020).
23. Andrews, T. *et al.* Accounting for Changing Temperature Patterns Increases Historical Estimates of Climate Sensitivity. *Geophys. Res. Lett.* (2018). doi:10.1029/2018GL078887
24. Armour, K. C. Energy budget constraints on climate sensitivity in light of inconstant climate feedbacks. *Nat. Clim. Chang.* (2017). doi:10.1038/nclimate3278
25. Hartmann, D. L. *et al. 2013: Observations: Atmosphere and Surface. In: Climate Change 2013: The Physical Science Basis. Contribution of Working Group I to the Fifth Assessment Report of the Intergovernmental Panel on Climate Change [Stocker, T.F., D. Qin, G.-K. Plattner, M. Tig* (2013). doi:10.1017/CBO9781107415324.008
26. Armour, K. C., Marshall, J., Scott, J. R., Donohoe, A. & Newsom, E. R. Southern Ocean warming delayed by circumpolar upwelling and equatorward transport. *Nat. Geosci.* (2016). doi:10.1038/ngeo2731
27. Gjermundsen, A. *et al.* Southern Ocean convection shutdown may hide potential for long-term climate warming by greenhouse gases. *Nature* Submitted (2020).
28. Parkinson, C. L. A 40-y record reveals gradual Antarctic sea ice increases followed by decreases at rates far exceeding the rates seen in the Arctic. *Proc. Natl. Acad. Sci. U. S. A.* (2019). doi:10.1073/pnas.1906556116
29. Lenssen, N. J. L. *et al.* Improvements in the GISTEMP Uncertainty Model. *J. Geophys. Res. Atmos.* (2019). doi:10.1029/2018JD029522
30. GISTEMP, T. GISS Surface Temperature Analysis (GISTEMP), version 4. *NASA Goddard Institute for Space Studies. Dataset accessed 2020-04-03* Available at: https://data.giss.nasa.gov/gistemp/.
31. Forster, P. M. *et al.* Evaluating adjusted forcing and model spread for historical and future scenarios in the CMIP5 generation of climate models. *J. Geophys. Res. Atmos.* (2013). doi:10.1002/jgrd.50174
32. Andrews, T., Gregory, J. M. & Webb, M. J. The dependence of radiative forcing and feedback on evolving patterns of surface temperature change in climate models. *J. Clim.* (2015). doi:10.1175/JCLI-D-14-00545.1
33. Austin, R. T., Heymsfield, A. J. & Stephens, G. L. Retrieval of ice cloud microphysical parameters using the CloudSat millimeter-wave radar and temperature. *J. Geophys. Res.*

Atmos. (2009). doi:10.1029/2008JD010049
34. Deng, M., MacE, G. G., Wang, Z. & Okamoto, H. Tropical composition, cloud and climate coupling experiment validation for cirrus cloud profiling retrieval using cloudsat radar and CALIPSO lidar. *J. Geophys. Res. Atmos.* (2010). doi:10.1029/2009JD013104
35. Deng, M., Mace, G. G., Wang, Z. & Berry, E. Cloudsat 2C-ICE product update with a new Ze parameterization in lidar-only region. *J. Geophys. Res.* (2015). doi:10.1002/2015JD023600